Evaluation of Thermal Breakage in Bimetallic Work Roll Considering Heat Treated Residual Stress Combined with Thermal Stress during Hot Rolling

Kejun Hu, Yongmei Xia, Fuxian Zhu, and Nao-Aki Noda*

Bimetallic rolls are widely used in steel rolling industry because of their excellent hardness, wear resistance, and high temperature properties. Heat treated residual stresses consist of compressive stress in the shell and tensile stress in the core are produced in the bimetallic roll during heat treatment. In the subsequent hot rolling process, severe thermal stresses are caused by heating-cooling thermal cycles at the roll surface. The combination of heat treated residual stresses and thermal stresses will cause a complex stress field in work roll during hot rolling process. The high combined tensile stress at the roll center may cause thermal breakage, once the tensile stress exceeds the material strength. Consequently, it is necessary to investigate the combined stresses to improve roll service life during hot rolling process. In this paper, the combined stresses in the work roll during hot rolling are investigated based on the FEM simulation, considering the heat treated residual stress after tempering process and thermal stress generated during hot rolling. In addition, the thermal breakage of work roll is evaluated in breakdown of water cooling systems and rolling incidents.

1. Introduction

Work roll is one of the most important tools for hot and cold forming to reduce the thickness of metal stock. The shape profile and surface quality of a work roll can largely determine the quality of products and productivity. Considerable residual stresses, namely, heat treated residual stress, are caused by temperature gradient and phase transformation during heat treatment process including quenching and tempering processes. The compressive heat treated residual stresses in the shell and the tensile heat treated residual stresses in the core are produced in the bimetallic work roll after heat treatment. In the subsequent hot rolling process, work rolls are subject to the cyclic sequence of heating-cooling over the roll surface due to contact with hot strip and following water cooling during every hot rolling revolution. Hence, large thermal gradient occurs near the surface, resulting in severe stresses named thermal stresses in work roll. The thermal stresses will cause some surface damages, such as wear, crack, and spalling.[1–4] Moreover, another form of roll fracture known as thermal breakage originates near the roll center and spreads to the surface. The thermal breakage is closely related to the thermal stresses at the roll center. Consequently, considerable effort has been devoted to investigate thermal behavior of work roll.

In addition, the combination of heat treated residual stresses and thermal stresses will cause a complex stress field in work rolls during hot rolling process.[5–7] Thus, this study uses combined stress to represent the stresses during hot rolling to distinguish from the pure thermal stress. Previous studies mainly focused on surface stresses including thermal stress and the mechanical stress, however, few were on center stresses.[8–14] Meanwhile, few studies covered heat treated residual stress when dealing with the stresses in the work roll during hot rolling. In fact, the heat treated residual stresses in the work rolls significantly impacts the service life of work rolls. The compressive heat treated residual stresses can prevent thermal crack initiation at the roll surface, where subject to the cyclic sequence loads.[15] At the same time, the tensile heat treated residual stress will be added to the tensile thermal stress in the center. The combined tensile stress may induce thermal breakage at the roll center, once the tensile stress exceeds the material strength.[16,17] Therefore, it is essential to take the heat treated residual stress into consideration to investigate the thermal behavior and the failures of work rolls.

In our previous studies,[18,19] the quenched residual stresses generation mechanism of work roll during quenching has been investigated considering the influence factors, such as, expansion value accompanied by phase transformation, shell-core ratio, diameter, creep behavior, and a new quenching method named non-uniform heating quenching. However, the quenching temperature and the subsequent tempering process have not been studied yet. The quenching temperature has a significant influence on the structure and properties of high speed steel (HSS) rolls.[20,21] Therefore, the effect of quenching temperature on residual stress should be discussed. Moreover, the quenched residual stress will be released during tempering process. Thus, before the simulation of hot rolling, the tempering process should be conducted to raise the simulation accuracy.

K. Hu, Y. Xia, F. Zhu, N.-A. Noda
School of Materials and Engineering, Jiangsu University of Technology, Changzhou, Jiangsu, 213001, China
E-mail: Kejun1004@126.com

DOI: 10.1002/srin.201700368

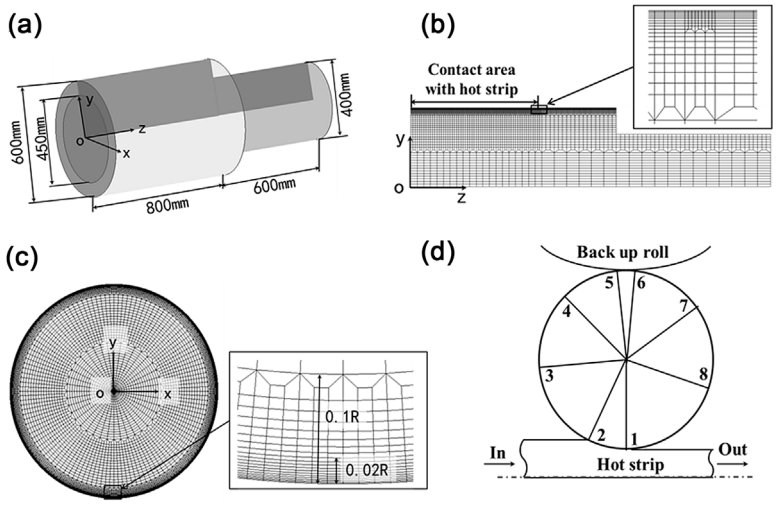

Figure 1. Bimetallic work roll and FEM model: a) Schematic diagram of bimetallic work roll, b) FEM model in the axial plane c) FEM model in the cross-section plane and d) Thermal boundary conditions at the roll surface during hot rolling.

In this paper, the evaluation of thermal breakage of bimetallic work roll will be performed using a finite element method (FEM), focusing on the combined stress at the roll center. First, the simulations considering quenching temperature and tempering process will be performed. Subsequently, simulation of hot rolling will be performed to obtain the temperature in the work roll, considering thermal conditions including hot strip contact, water cooling, wiper cooling, and air cooling. Afterward, the combined stress will be carried out using a thermo-elastic model and combine with the heat treated residual stress. At last, the thermal breakage of work roll will be evaluated using the combined stresses at the roll center in breakdown of water cooling systems and rolling incidents.

2. FEM Simulations

2.1. Bimetallic Work Roll and FEM Model

The bimetallic work roll is manufactured by centrifugal casting method, using high speed steel (HSS) as shell material and the ductile casting iron (DCI) as core material. As shown in **Figure 1**a, the roll diameter is 600 mm, with the body length of 1600 mm, and the shell thickness of 75 mm. The chemical compositions of HSS and DCI of the bimetallic work roll and the experimentally measured material properties at room temperature are given in **Table 1** and **2**, respectively.

In order to reduce the total computational effort and save time, two simplified models are used, consisting of a FEM model in the axial plane shown in Figure 1b and a FEM model in the cross section plane shown in Figure 1c of work roll. The FEM model in the axial plane is used for the simulation of heat treated residual stress during heat treatment and the simulation of combined stress during hot rolling. The FEM model in the cross section plane is used for the simulation of temperature during hot rolling. As shown in Figure 1b, a mesh refinement is considered near the roll surface with very large thermal gradient during hot rolling, especially near the contact area with hot strip. At the same time, a mesh refinement is imposed near the roll surface, in both tangential and radial directions, as shown in Figure 1c.

2.2. FEM Analysis for Heat Treatment

In this paper, the simulation of heat treated residual stress considering quenching temperature and tempering process, will be performed using the FEM model in the axial plane in Figure 1b.

Similar to the experimental procedure and simulation method in our previous studies,[18] the experimentally measured surface temperature is imposed on the roll surface of the FEM model. Furthermore, the material properties of HSS and DCI were measured experimentally depending on temperature including room temperature and 100–1100 °C with an interval of 100 °C. Afterward, the obtained material properties are applied to the simulation as input data. Finally, it should be noted that this paper uses dimensionless time to avoid the disclosure of heat treatment process.

2.3. FEM Analysis for Hot Rolling

After the heat treatment, the simulation of hot rolling of will be performed. Firstly, the temperature simulation will be performed using the FEM model in Figure 1c. Then, the combined

Table 1. Chemical compositions of high speed steel and ductile casting iron for high speed steel roll /mass%.

Composition	C	Si	Mn	P	S	Ni
HSS	1–3	< 2	< 1.5			< 5
DCI	2.5–4	1.5–3.1		< 0.1	< 0.1	0.4–5
	Cr	Mo	Co	V	W	Mg
	2–7	< 10	< 10	3–10	< 20	< 10
	0.01–1.5	0.1–1				0.02–0.08

Table 2. Mechanical and thermal properties of high speed steel and ductile casting iron for high speed steel roll at room temperature.

Property	HSS	DCI
0.2% proof stress [MPa]	1282	415
Young's modulus [GPa]	210	173
Poisson's ratio	0.3	0.3
Density [kg m^{-3}]	7600	7300
Thermal expansion coefficient [K^{-1}]	12.6×10^{-6}	13.0×10^{-6}
Thermal conductivity [W/(m · K)]	20.2	23.4
Specific heat [J/(kg · K)]	461	460

stress simulation will be performed using the FEM model in Figure 1b.

The thermal behavior of work roll during the stable rolling condition has been reported by many researchers, therefore, this paper focus on the early stage of the first stand of hot strip finishing rolling. In addition, the high risk of thermal breakage occurs in the early stage of hot rolling due to the lower temperature in the roll core and the higher temperature in the roll shell.[16] In this paper, a uniform temperature is assumed as 30 °C in the work roll before rolling. Figure 1d shows the thermal boundary conditions along the θ-direction of the work roll during one rolling revolution in this paper. Arc 1–2 indicates the contact zone between work roll and hot strip; Arc 2–3 and 8–1 indicate the wiper cooling zones; Arc 3–4 and 7–8 indicate the water spraying zones; Arc 4–5 and 6–7 indicate the natural air cooling zones; and arc 5–6 indicates the contact zone between work roll and backup roll. The above thermal boundary conditions are imposed on the roll surface. It should be noted that the heat generated by strip deformation and the mechanical loads are not taken into account in this paper. Further, to shorten the computational effort and save time, work roll rotation has been simulated by fixed roll and rotating thermal loadings on its boundary.[22,23] In fact, the hot rolling parameters strongly influence work roll temperature, including initial temperature of work roll and hot strip, material properties of work roll and hot strip, the nozzle spraying cooling condition (such as nozzle pressure, nozzle flow, nozzle position, and angle even the distance from work roll surface), the oxidation layer, and so on.[13,14,24] The effects of these parameters on the work roll temperature can be presented by the heat transfer coefficients. Since the heat transfer coefficients are very complicated and difficult to be obtained, the available reports on the heat transfer coefficients of work roll are always different with each other. With regard to HSS work roll, the different heat transfer coefficients can be found changed in a large range even only the heat transfer coefficient of water cooling.[14,25] However, it should be noted that this paper aims to provide a model to clarify the thermal breakage caused by combined stress. Especially, the combined stress occurs in the roll center, which has not been discussed yet. The heat transfer coefficients are adopted in the analysis, as shown in **Table 3** although difference may exist compared with the actual heat transfer coefficients. Meanwhile, the heat transfer coefficients varying in a wide range are designed to evaluate the effect of heat transfer coefficients on combined stresses in the roll center.

Table 3. Industrial rolling parameters used in the FEM simulation.

Parameter		Value
Velocity of work roll [m s^{-1}]		1.51
Rolling pressure[kN]		15 390
Initial work roll temperature [°C]		30
Hot strip material		SS400
Strip width [mm]		1000
Strip thickness at entrence [mm]		40
Rolling reduction		41.7%
Entry strip temperature [°C]		1000
Air temperature [°C]		30
Water temperature [°C]		25
Water pressure [MPa]		1.3
Heat transfer coefficient [kW/(m^2 · K)][19]	Bite heating	49.5
	Wiper cooling	15
	Water cooling	35
	Air cooling	0.005

3. Results and Discussion of Heat Treated Residual Stress during Heat Treatment

3.1. Effect of Quenching Temperatures on Residual Stress

As shown in **Figure 2**a, in order to investigate the effect of quenching temperature, a higher quenching temperature $T_{\mathrm{High}} = 1100\,^{\circ}\mathrm{C}$ and a lower quenching temperature $T_{\mathrm{Low}} = 1000\,^{\circ}\mathrm{C}$ are designed to compare with the conventional quenching temperature $T_{\mathrm{Conventional}} = 1060\,^{\circ}\mathrm{C}$ of HSS work roll. Meanwhile, the surface cooling speeds of three quenching processes are consistent.

As shown in Figure 2b, at the end of quenching processes, both center tensile stresses and surface compressive stresses increase with increasing quenching temperature. As shown in the local amplification in Figure 2b, the stresses of three quenching processes are similar before the core pearlite transformation. However, the decrement of center residual stress decreases with increasing of quenching temperature, when the pearlite transformation starts from shell-core boundary. To balance the center stress, the decrement of surface stress also decreases with increasing of quenching temperature. After the center pearlite transformation, the stress changes both surface and center are almost the same. As a result, the final center residual stress decreases with increasing quenching temperature. The reason for the final center stress decrease can be concluded as the center cooling speeds are different for three quenching processes although the surface cooling speeds are consistent. As shown in the local amplification in Figure 2a, the center cooling speed increases with increasing quenching temperature before the pearlite transformation. Meanwhile, the center cooling speeds are the same after pearlite transformation.

As shown in Figure 2c, compared with the residual stress 376 MPa at the roll center in the conventional quenching temperature $T_{\mathrm{Conventional}}$, the residual stress increases by 8.9% from 376 to 413 MPa in the higher quenching temperature T_{High}. At the same time, the residual stress decreases by 14.9% from 376 to 320 MPa in the lower quenching temperature T_{Low}.

3.2. Heat Treated Residual Stress after Tempering Process

The tempering process will be conducted for a bimetallic work roll after quenching to obtain the stable microstructure and release the quenched residual stress. As shown in **Figure 3**, after the quenching process published in the previous study,[18] the roll is slowly heated up to $T_{\mathrm{Temperting}}$ and kept at $T_{\mathrm{Temperting}}$ for

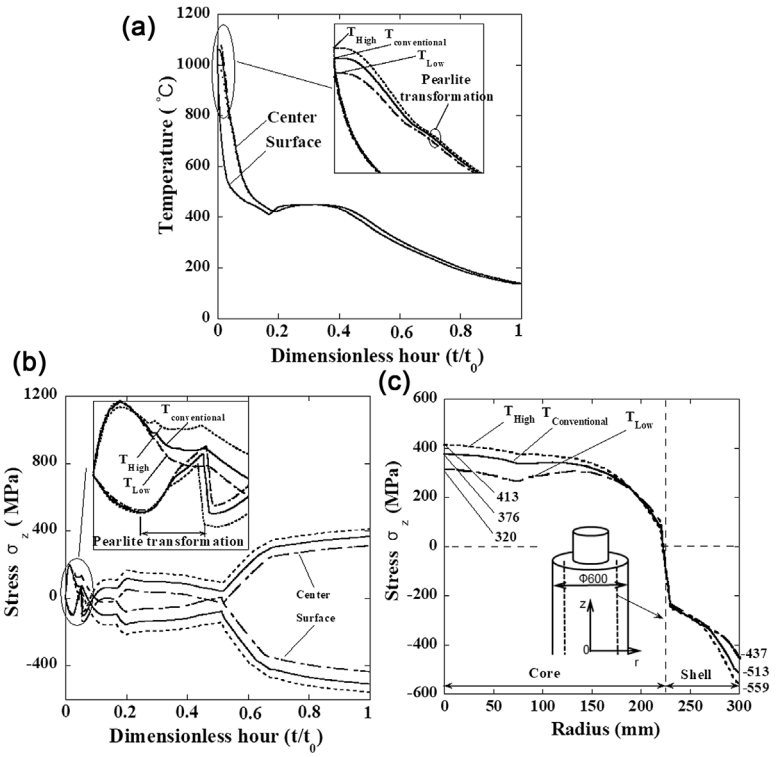

Figure 2. Residual stress distribution in different quenching temperatures: a) Temperature histories, b) Residual stress σ_z histories, c) Residual stress σ_z distributions along the axial direction.

several hours. Then, the roll is slowly cooled down to room temperature. It should be noted that the tempering process will be repeated for two times in this study.

In this paper, the heat treated residual stress after tempering will be applied to the subsequent thermal stress simulation as the initial stress. However, since the tempering process is one of the important process parameters for the residual stress in the bimetallic roll, the tempering will be specially discussed in our further paper. Therefore, the tempered residual stress distribution would not be published in this paper to avoid prematurely revealing the results of tempering process discussed in the future paper. However, since this study focused on evaluating thermal breakage caused by the combined stress at the center, there is no effect on understanding of the final results.

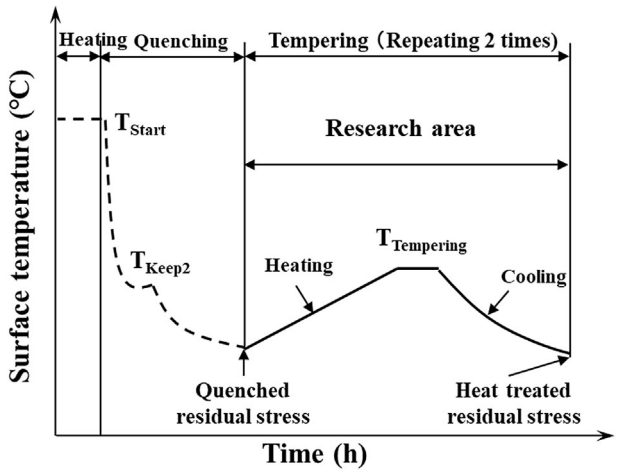

Figure 3. Schematic diagram of roll surface temperature during heat treatment.

4. Results and Discussion of Temperature and Combined Stress during Hot Rolling

4.1. Temperature in the Work Roll during Hot Rolling

In this section, the simulation of temperature in work roll during hot rolling will be performed. **Figure 4**a shows the temperature variation at the roll surface during the first rolling revolution. It is seen that surface temperature rapidly rises to the peak value of 573 °C in the bite zone from 1 to 2 due to contact with the hot strip. Compared to the results in previous studies focusing on the HSS work roll at the F1 stand of hot strip rolling, the peak temperature 573 °C in this study is relatively small but in reasonable range. For example, the peak temperature reaches 581.3 °C in ref.[14] and reaches 582.5 ° in ref.[25] after the first rolling revolution. The differences between this study and references can be caused by rolling speed, strip contact time and initial roll or strip temperature. Therefore, the results obtained in this simulation are available for evaluating the temperature in HSS work roll during hot rolling. After the bite zone, the surface temperature rapidly drops due to the following wiper cooling from 2 to 3. After the wiper cooling, the surface temperature continues to drop in the water cooling zone from 3 to 4. Since the subsurface temperature is higher than the surface temperature, the heat transfers from the subsurface to the surface. As a result, the surface temperature slightly rises instead of continuously drops in the water cooling zone from 4 to 7. In the subsequent process from 7 to 1, the surface temperature gradually drops. After first rolling revolution, the surface temperature increases from the initial temperature 30–38 °C. In addition, in the second rolling revolution, the peak surface temperature increases to 576 °C in the bite region from 1 to 2.

Figure 4b shows the temperature history at the roll surface during one strip rolling process. The maximum surface temperatures are stable at 583 °C after 5 rolling revolutions. Figure 4c shows the temperature histories near the roll surface during one strip rolling process, considering different depths (including $r/R = 0.995, 0.99, 0.98, 0.95$) along radial direction. In this study, R is the radius of HSS work roll and r is the distance from the roll center. In order to clearly display the temperature variation near the roll surface, the historical process 5.5–75.5 s is not shown in the Figure 4c. Compared with the surface temperature variation during hot rolling, the temperature increment is smaller in the subsurface of the work roll and

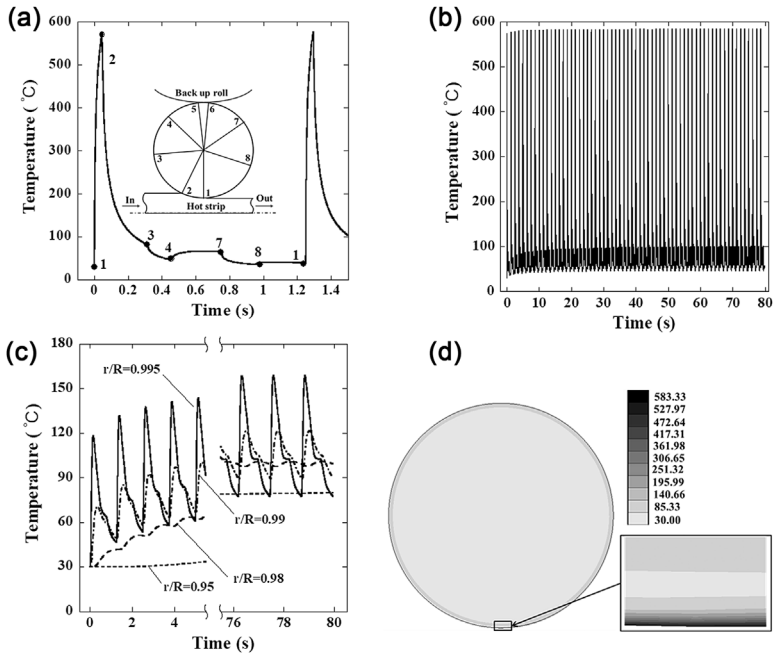

Figure 4. Temperature field in the work roll during hot rolling: a) Temperature distributions at the roll surface during the first rolling revolution, b) Temperature history at the roll surface during one strip rolling process, c) Temperature histories near the roll surface during one strip rolling process, d) Temperature contour of the work roll at the end of a strip rolling process.

the maximum temperature decreases with increasing depth. It is confirms that great thermal gradient only appears in a small depth from the work roll surface. This phenomenon can be further indicated in the Figure 4d. As shown in Figure 4d, the thermal penetration depth is up to 45 mm.

4.2. Combined Stress in the Work Roll during Hot Rolling

In this part, the simulation of combined stress will be performed using FEM model in Figure 2b. The obtained surface temperature in Figure 4b is imposed on the roll surface. The heat treated residual stress after tempering process is applied to combined stress simulation as the initial stress. Since this paper mainly focuses on the combined stress at the roll center, a simple thermo-elastic analysis is performed. Thus, the plastic parameters including the yield stress and stress–strain curves are without considering in this simulation.

Figure 5 shows the combined stress σ_z history at the roll surface during a whole strip rolling process. The combined stress in Figure 5 consists of heat treated residual stress and thermal stress. Figure 5a shows the combined stress variation at the first rolling revolution. As shown in Figure 5a, since the surface temperature rises in the bite zone from 1 to 2, the large combined compressive stress σ_z generates and rapidly increases. Then, the combined compressive stress σ_z rapidly decreases from point 2 to point 4 due to the wiper cooling and water cooling. From 4 to 7, the combined compressive stress σ_z slightly increases due to the temperature rising. From 7 to 1, the combined compressive stress gradually decreases. It is seen that the change trend of combined stress is similar to the result of surface temperature.

It should be noted that the excessive peak value of combined stress reaches −2640 MPa at the first rolling revolution. The excessive combined compressive stress can be explained in the following two aspects. For one thing, the heat treated compressive residual stress considered in this study has not been taken into consideration in the ref.[14,22] If without considering the heated residual stress, the initial stress would be 0 at the start of the hot rolling. However, the heat treated residual stress at the roll surface is high enough after tempering process even though slightly decreases. Therefore, the generated thermal stress is only −2162 MPa included in the −2640 MPa during hot rolling. For another, this study applies thermo-elastic analysis instead of thermo-plastic-elastic analysis. The thermo-elastic stress generated in the roll surface can be evaluated through the following Equation 1.[26]

$$\sigma_z = \sigma_\theta = -\frac{aE(T_{\text{Surface}-}T_{\text{Core}})}{1-v}, \sigma_r = 0 \quad (1)$$

where T_{Surface} is surface temperature, T_{Core} is core temperature, a is thermal expansion coefficient, E is Young's modules, v is Poisson's ratio.

The thermo-elastic stresses are calculated with the Equation 1 when $T_{\text{Surface}} = 573\,^{\circ}\text{C}$, $T_{\text{Core}} = 30\,^{\circ}\text{C}$, $a = 12.6 \times 10^{-6}/\text{K}$, $E = 210\,\text{GPa}$, $v = 0.3$. The calculated thermo-elastic stresses are also indicated in Figure 5a to compare with the thermal stresses obtained in FEM simulation. Since the stress in Figure 5 consists of heat treated residual stress and the thermal stress, the same heat treated residual stresses are also added to the calculated thermo-elastic stresses in Figure 5a. It is found that the combined stress obtained in FEM simulation is well agreement with the calculated stress with the error of 5% for the maximum stress. The same error was also observed and explained in the ref.[23] Therefore, it is confirmed that the thermo-elastic analysis is able to predict the thermal stress although it cannot actually replace an elastic-plastic analysis. In addition, it also should be noted that tensile thermal stress does not occur because the roll center temperature is lower than roll surface temperature during early stage of hot strip rolling. Since only the early stage of hot strip rolling is investigated, the initial temperature of work roll is assumed as 30 °C. In fact, the work roll body temperature can reach to 100 °C during stable hot rolling condition.[14] According to the Equation 1, the tensile thermal stress will be generated when $T_{\text{Core}} > T_{\text{Surface}}$. The tensile-compressive stress cycle is one of the important parameters to predict fatigue life of work roll.[23,27] Therefore, the thermo-elastic-plastic behavior and the stable rolling will be carried out to evaluated fatigue life of work roll in the future study.

Figure 5b shows the combined stress variation at the roll surface during a whole strip rolling process. The surface maximum combined stress reaches −2650 MPa after five rolling revolutions. As have been discussed, the maximum combined stress −2650 MPa consists of heat treated residual stress and the

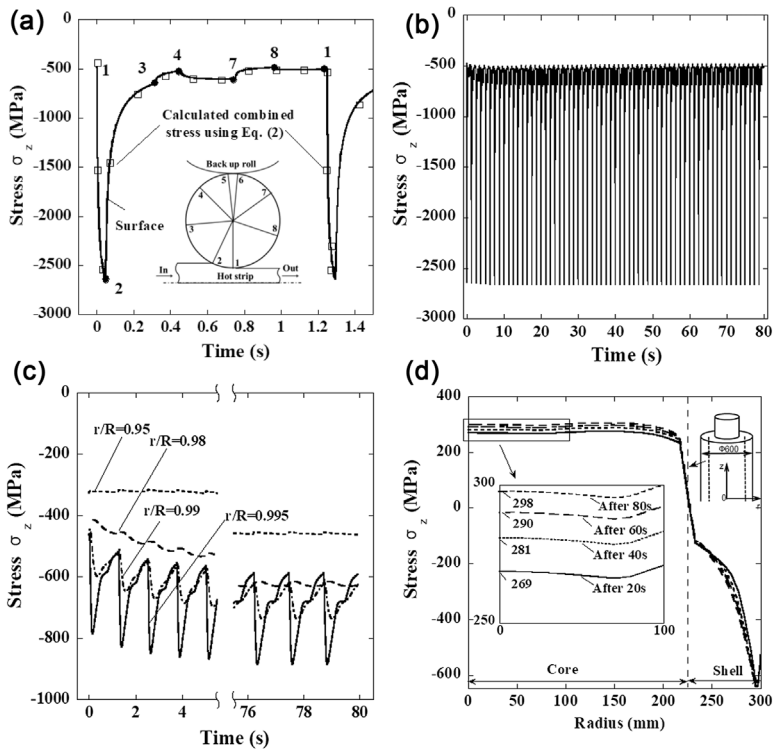

Figure 5. Combined stress σ_z field in the work roll during hot rolling: a) Combined stress σ_z distribution at the surface during the first rolling revolution, b) Combined stress σ_z history at the roll surface during one strip rolling process, c) Combined stress σ_z histoies near the roll surface, d) Combined stress σ_z distribution at the different rolling time.

thermal stress. Figure 5c shows the stress histories near the roll surface during one strip rolling process, considering different depths (including $r/R = 0.995$, 0.99, 0.98, 0.95) along radial direction. Similarly to temperature increment near the surface, the combined stress increment is smaller than the results at the surface. Figure 5d shows the stress σ_z distribution at different times during hot rolling process. It is seen that tensile stress at the roll center reaches 269 MPa after 20 s and increases to 297 MPa after 80 s during one strip rolling process. Therefore, the risk of thermal breakage near the roll center is relatively slight during the early stage of a normal hot rolling process compared with the core material strength 415 MPa. In addition, the compressive stress decreases near the surface due to the surface temperature is lower than subsurface temperature at the end of one rolling revolution.

In order to evaluate the effect of heat transfer coefficients on combined stresses in the roll center, the different heat transfer coefficients including h_{bite} in the roll bite region, h_{wiper} in the wiper cooling regions, and h_{water} in the water spraying cooling regions are discussed. **Table 4** shows the heat transfer coefficient considered in this study and the combined stresses at the roll center and surface after 80 s. As shown in Table 4, similar to the results in refs.,[13,14] the heat transfer coefficients has an significant effect on the maximum surface temperature. However, the combined stresses in the roll center and surface are almost unchanged with the different heat transfer coefficients. Therefore, it is confirmed that the heat transfer coefficients has a small effect on combined stresses in the roll center during the early stage of hot rolling.

5. Evaluation of Thermal Breakage in the Work Roll during Hot Rolling

Thermal breakage in the work roll is closely related to the maximum temperature difference between the roll surface and the roll center. The high temperature difference may be induced by a high heating rate at the roll surface due to poor water cooling systems, breakdown of water cooling systems, or high throughput at the beginning of the rolling campaign. Worse still, in some rolling accidents, the blocked or piled up strip would result to the stoppage of rolling and the local overheat of roll surface. In the abnormal hot rolling mentioned before, high tensile thermal stresses would occur at the roll center. At the same time, tensile heat treated residual stress is added to tensile thermal stress at the roll center to form the combined stress. When the combined tensile stress exceeds the material strength, the thermal breakage of work roll may occur abruptly. It has been confirmed that the combined stress 297 MPa during the early

Table 4. Effects of heat transfer coefficient on combined stresses at the roll center and surface.

	Heat transfer coefficient ($kW\,m^{-2}\cdot K$)				Maximum surface temperature (°C)	Combined stress σ_z after 80 s (MPa)	
Simulations	h_{bite}	h_{water}	h_{wiper}	h_{air}	T_{max}	σ_{center}	$\sigma_{surface}$
1	49.5	35	15	0.005	583	298	−522
2	55	35	15	0.005	604	305	−532
3	45	35	15	0.005	556	289	−508
4	49.5	40	15	0.005	578	291	−507
5	49.5	30	15	0.005	579	293	−513
6	49.5	35	20	0.005	577	286	−492
7	49.5	35	10	0.005	581	300	−526

stage of a normal hot rolling is much less than the core material strength. Therefore, the thermal breakage is discussed in the abnormal hot rolling conditions.

In this study, abnormal hot rolling conditions will be divided into breakdown of water cooling systems and rolling accidents. First, simulation of water cooling systems breakdown simply applies hot strip contact and air cooling into thermal boundary conditions. Second, the simulation of rolling accidents applies hot strip contacts as the thermal boundary conditions. The simulation time in the two cases is 80 s, which is the time for a complete strip rolling process.

Figure 6a shows the temperature variations at the roll surface and the depth of $r/R = 0.95$ in both the breakdown of roll cooling systems and rolling incidents. As shown in Figure 6a, the peak roll surface temperatures rises over the rolling time with unstable maximum temperature in the breakdown of water cooling systems. In contrast, the surface temperature increment decreases over the rolling time. At the end of hot rolling, the maximum temperature reaches 774 °C at the roll surface and 356 °C at the depth of $r/R = 0.95$. In the rolling incidents, the surface temperature rises significantly until the maximum temperature reaches 951 °C and the temperature at the depth of $r/R = 0.95$ gradually rises until the maximum temperature is up to 402 °C. In abnormal hot rolling process, both surface and subsurface temperature rise significantly and the thermal penetration depth can be up to 100 mm. However, the temperature near the roll center is almost unchanged at the initial temperature 30 °C. Hence, based on Figure 6a, temperature differences have been notably wider during abnormal hot rolling processes.

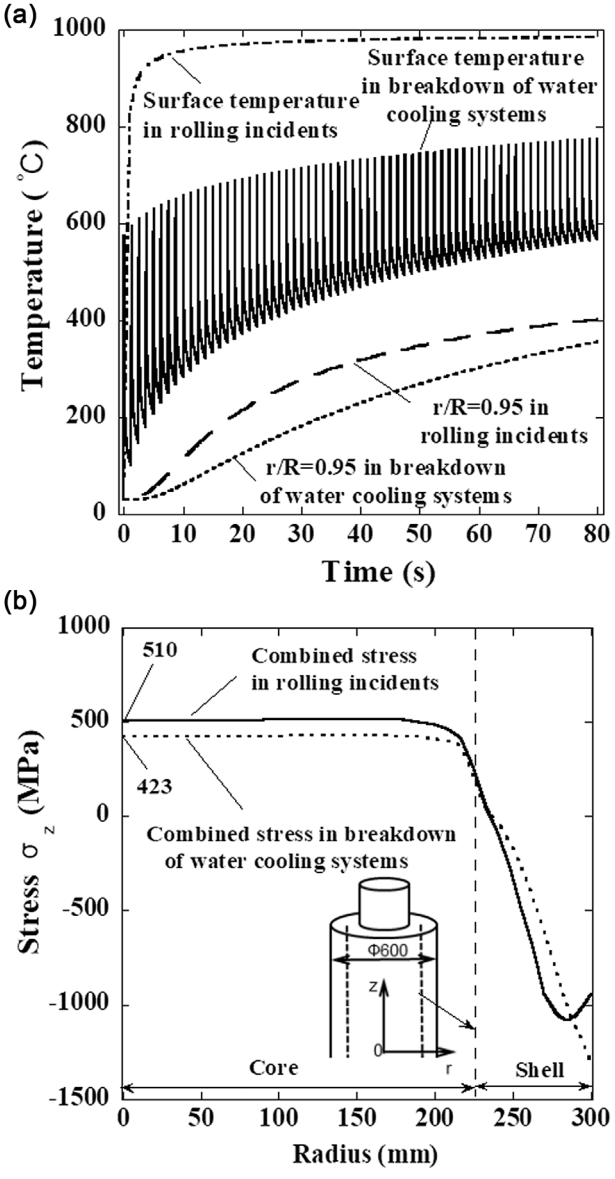

Figure 6. Evaluation of thermal breakage of work roll during abnormal hot rolling: a) Temperature histories at the roll surface and at the depth of $r/R = 0.95$ in breakdown of water cooling systems and rolling incidents, b) Combined stress σ_z distributions.

Figure 6b shows the comparison of combined stress distributions in abnormal hot rolling processes. The tensile combined stress at the roll center is up to 423 MPa in the breakdown of roll cooling systems and reaches 510 MPa in the rolling incidents. Compared with the core material strength 415 MPa, the combined tensile stresses (423 MPa or 510 MPa) will cause thermal breakage. Therefore, the thermal breakdown of work roll will abruptly occur if the breakdown of cooling systems or rolling incidents is not found timely.

6. Conclusions

In this paper, the evaluation of thermal breakage of bimetallic work roll during the early stage of hot strip rolling was performed based on the FEM simulation. The combined stresses were predicted considering the heat treated residual stress after tempering and the thermal stress during hot rolling. In addition, this paper discussed the impacts of heat coefficients and abnormal hot rolling on combined stresses. The results of the current study can be summarized as follows:

1) Compared with the result in the conventional quenching temperature $T_{\text{Conventional}}$, the center residual stress increases by 8.9% in the higher quenching temperature T_{High} and decreases by 14.9% in the lower quenching temperature T_{Low}.
2) The surface temperature rapidly rises in the bite region and rapidly drops in the subsequent wiper and water cooling. The maximum surface temperatures were stable at 583 °C after five rolling revolutions, while there is no stable maximum temperature at the subsurface.
3) The simulation results of thermo-elastic stresses at the roll surface agree with the calculation results using Equation 1. The combined tensile stress reaches 297 MPa at the roll center during a normal strip rolling process. The heat transfer coefficients have a very small effect on combined stress in the roll center.
4) The combined tensile stresses at the roll center significantly increase due to the wider temperature difference during abnormal hot rolling processes. The combined tensile stresses at the roll center can cause thermal breakage in work roll.

Keywords

FEM, hot rolling, residual stress, thermal stress, work roll

Received: August 27, 2017
Revised: October 25, 2017
Published online: November 20, 2017

[1] N. F. Garza-Montes-De-Oca, W. M. Rainforth, *Wear* **2009**, *267*, 441.
[2] R. D. Mercado-Solis, J. Talamantes-Silva, J. H. Beynon, M. A. L. Hernandez-Rodriguez, *Wear* **2007**, *263*, 1560.
[3] R. D. Mercado-Solis, J. H. Beynon, *Scand. J. Metall.* **2010**, *34*, 175.
[4] R. Colás, J. RamíRez, I. Sandoval, J. C. Morales, L. A. Leduc, *Wear* **1999**, *230*, 56.
[5] Y. Sano, K. Kimura, *Tetsu- to- Hagane* **1987**, *73*, 1154.
[6] C. F. Onisa, D. C. J. Farrugia, *Int. J. Mater. Form.* **2008**, *1*, 363.
[7] M. Hinnemann, P. J. Mauk, V. Goryany, C. Zybill, R. Braun, *Key Eng. Mater.* **2014**, *622*, 949.
[8] R. M. Guo, *Trans. ASME J. Manuf. Sci. Eng.* **1998**, *120*, 28.
[9] C. S. Li, X. H. Liu, G. D. Wang, X. M. He, *Mater. Sci. Technol.* **2013**, *18*, 1147.
[10] J. D. Lee, M. T. Manzari, Y. L. Shen, W. Zeng, *Trans. ASME J. Manuf. Sci. Eng.* **2000**, *122*, 706.
[11] D. Benasciutti, E. Brusa, G. Bazzaro, *Procedia Eng.* **2010**, *2*, 707.
[12] A. Sonboli, S. Serajzadeh, *Mater. Sci. Technol.* **2013**, *26*, 343.
[13] G. Y. Deng, H. T. Zhu, A. K. Tieu, Q. Zhu, L. H. Su, M. Reid, P. T. Wei, L. Zhang, H. Wang, J. Zhang, J. T. Li, T. D. Ta, Q. Wu, *Mater. Sci. Forum* **2017**, *904*, 55.
[14] G. Y. Deng, H. T. Zhu, A. K. Tieu, L. H. Su, M. Reid, L. Zhang, P. T. Wei, X. Zhao, H. Wang, J. Zhang, J. T. Li, T. D. Ta, Q. Zhu, C. Kong, Q. Wu, *Int. J. Mech. Sci.* **2017**, *131–132*, 811.
[15] Y. Sano, T. Hattori, M. Haga, *ISIJ Int.* **1992**, *32*, 1194.
[16] K. H. Schroder, *A Basic Understanding of the Mechanics of Rolling Mill Rolls*, Eisenwerk Sulzau-Werfen, ESW-Handbook, Tenneck, Austria **2003**, p. 71.
[17] CAFE, *Roll Failures Manual: Hot Mill Cast Work Rolls*, The European Foundry Association, Roll Section, Düsseldorf, German **2002**, p. 19.
[18] N.-A. Noda, K. Hu, Y. Sano, K. Ono, Y. Hosokawa, *Steel Res. Int.* **2016**, *87*, 1478.
[19] N.-A. Noda, K. Hu, Y. Sano, K. Ono, Y. Hosokawa, *Steel Res. Int.* **2016**, *83* DOI: 10.1002/srin.201600165.
[20] H. G. Fu, H. J. Zhao, Z. Z. Du, Z. J. Feng, Y. P. Lei, Y. Zhang, M. W. Li, Y. H. Jiang, R. Zhou, H. X. Guo, *Ironmaking Steelmaking* **2011**, *38*, 338.
[21] H. G. Fu, X. L. Chen, Z. Z. Du, Y. P. Lei, Z. J. Feng, *China Foundry* **2009**, *6*, 15.
[22] G. Y. Deng, Q. Zhu, K. Tieu, *J. Mater. Process. Technol.* **2017**, *240*, 200.
[23] D. Benasciutti, *J. Strain Anal. Eng. Des.* **2012**, *47*, 297.
[24] S. Serajzadeh, *Int. J. Adv. Des. Manuf. Technol.* **2008**, *35*, 859.
[25] J. H. Gao, C. Q. Huang, M. Wang, J. P. Huang, *Mater. Mech. Eng.* **2009**, *33*, 46.
[26] S. Timoshenko, J. N. Goodier. *Theory of Elasticity*, McGraw-Hill, New York **1951**.
[27] M. Raudensky, J. Horsky, J. Ondrouskova, B. Vervaet, *Steel Res. Int.* **2013**, *84*, 269.

